Deflection flows ahead of ICMEs as an indicator of curvature and geoeffectiveness

Y. Liu,[1,2] W. B. Manchester IV,[3] J. D. Richardson,[4,2] J. G. Luhmann,[1] R. P. Lin,[1] and S. D. Bale[1]

Received 19 December 2007; revised 24 April 2008; accepted 5 May 2008; published 18 July 2008.

[1] We examine the upstream meridional deflection flows of interplanetary coronal mass ejections (ICMEs) in an effort to investigate their cross-sectional shape and the magnetic field orientation in their sheath regions. Eight out of 11 magnetic clouds (MCs) near solar minimum identified for the curvature study are concave outward as indicated by the elevation angle of the MC normal with respect to the solar equatorial plane; an inverse correlation is observed between the meridional deflection flow and the spacecraft latitude for these concave-outward MCs, which suggests that the upstream plasma is deflected toward the equatorial plane. MHD simulations, however, show that the meridional deflection flow moves poleward for a concave-outward CME. The poleward flow deflection is observed only ahead of convex-outward MCs. Possibilities leading to this discrepancy are discussed. The deflection flow speed in sheath regions of ICMEs increases with the ICME speed relative to the ambient solar wind, which together with the coupling between the meridional magnetic field and deflection flow yields a positive linear correlation between the sheath meridional field and the ICME relative speed. This empirical relationship could predict the sheath meridional field based on the observed CME speed, which may be useful for space weather forecasting as ICME sheaths are often geoeffective. Implications of the deflection flows and ICME curvature are also discussed in terms of magnetic reconnection and particle acceleration in ICME sheaths.

Citation: Liu, Y., W. B. Manchester IV, J. D. Richardson, J. G. Luhmann, R. P. Lin, and S. D. Bale (2008), Deflection flows ahead of ICMEs as an indicator of curvature and geoeffectiveness, *J. Geophys. Res.*, *113*, A00B03, doi:10.1029/2007JA012996.

1. Introduction

[2] While coronal mass ejections (CMEs) and their interplanetary manifestations (ICMEs) have been studied by remote sensing and in situ measurements for more than 30 years, their global morphology and propagation in interplanetary space are still not well understood. Our current understanding about the global structure is a magnetic flux rope which remains connected to the Sun as ICMEs move in the ambient solar wind [e.g., *Burlaga et al.*, 1981]. Real ICMEs could have a more complicated topology due to their interaction with the ambient medium. The STEREO spacecraft are expected to shed light on the three-dimensional (3-D) morphology, providing both white light imaging and in situ measurements at two points widely separated in longitude [*Kaiser*, 2005]. The white light, or the photospheric radiation Thomson-scattered by electrons, essentially reflects a density structure, so the heliospheric image of ICMEs at large distances could be a density-enhanced region upstream of ICMEs owing to their compression; in situ observations at additional points still cannot give a full picture of ICMEs. Models are therefore needed even in the STEREO era.

[3] Various flux rope fitting models, either force-free [e.g., *Lepping et al.*, 1990; *Vandas and Romashets*, 2003] or non-force-free [e.g., *Mulligan and Russell*, 2001; *Hidalgo et al.*, 2002; *Cid et al.*, 2002; *Hu and Sonnerup*, 2002], have been developed to invert the global structure of ICMEs, or their subset, magnetic clouds (MC). MCs are characterized by a smooth and strong magnetic field, a large rotation in the field direction, and a low proton temperature [*Burlaga et al.*, 1981]. Tests of these flux rope fitting techniques using magnetohydrodynamic (MHD) simulations show that they are useful in determining the local axis orientation of MCs, but the true dimension and thus the magnetic flux content of MCs may be significantly underestimated [*Riley et al.*, 2004]. Direct evidence obtained from multiple spacecraft observations also shows that the transverse size of the MC cross section is much larger than the radial width [*Liu et al.*, 2006c], so MCs or common ICMEs are highly flattened. Understanding of the realistic picture of ICMEs, consistent with STEREO in situ measurements and wide angle coronagraph images, requires more sophisticated models.

[1]Space Sciences Laboratory, University of California, Berkeley, California, USA.
[2]State Key Laboratory of Space Weather, Chinese Academy of Sciences, Beijing, China.
[3]Center for Space Environment Modeling, University of Michigan, Ann Arbor, Michigan, USA.
[4]Kavli Institute for Astrophysics and Space Research, Massachusetts Institute of Technology, Cambridge, Massachusetts, USA.

0148-0227/08/2007JA012996

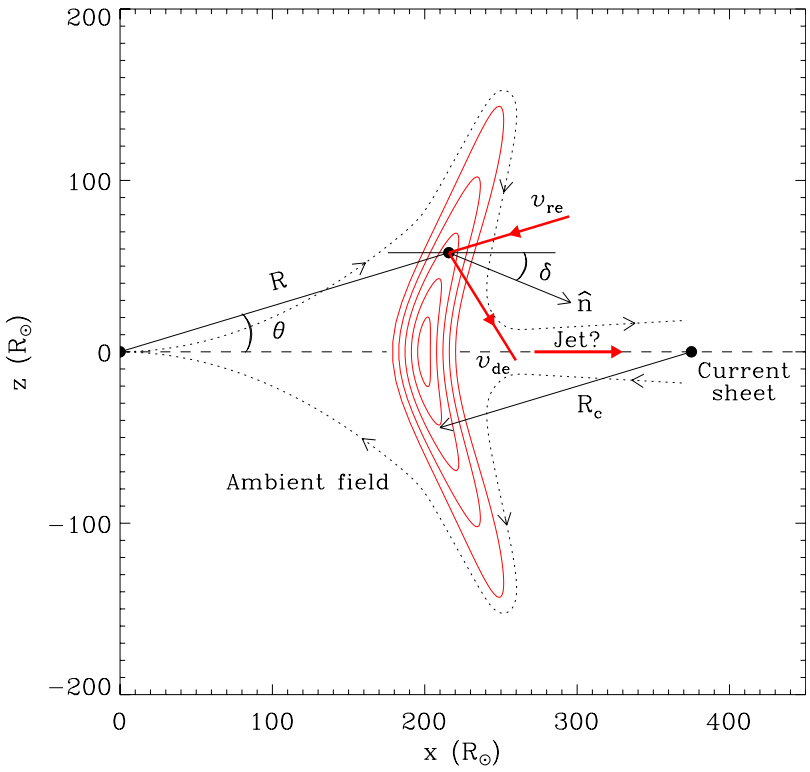

Figure 1. Schematic diagram of a magnetic cloud (MC) at 1 AU in the solar meridional plane with axis perpendicular to the radial and transverse directions, illustrating the curvature and consequent deflection flow (corresponding to solar minimum). The angles, labeled as θ and δ, represent the latitude of a virtual spacecraft and the elevation angle of the flux rope normal with respect to the equatorial plane. Dotted lines indicate the ambient magnetic field and dashed lines denote the current sheet. The distance of the spacecraft and the radius of curvature are marked as R and R_c, respectively. The incoming and deflected flows relative to the MC are denoted by v_{re} and v_{de}. Reproduced from paper 1.

[4] Global MHD modeling of ICME propagation in a uniform [e.g., *Odstrcil et al.*, 2002; *Riley et al.*, 2003] or structured [e.g., *Groth et al.*, 2000; *Odstrcil et al.*, 2004; *Manchester et al.*, 2004] solar wind provides a powerful tool for interpreting the observations, and is considered to be superior to flux rope fitting techniques [e.g., *Riley et al.*, 2004]. Certain restrictions also apply to these MHD simulations. First, the ICME plasma is collision dominated and magnetic dissipation is likely to occur [*Liu et al.*, 2006a], so the ideal MHD simulations are unable to describe the thermodynamic state of the ICME plasma. Second, in situ measurements along a one-dimensional (1-D) cut through the 3-D structure of an ICME can hardly give strong constraints on the MHD simulations. Important questions remain unanswered regarding how well the MHD simulations can reproduce the ambient solar wind state and the interaction between ICMEs and the ambient medium.

[5] *Liu et al.* [2006c, hereinafter referred to as paper 1] present a new technique to investigate the curvature of the MC cross section resulting from the distortion by the ambient solar wind. Figure 1 shows an idealized sketch of a flux rope cross section spanning an angle of 60° in the solar meridional plane. If a CME at solar minimum emerges from a helmet streamer by stressing the closed magnetic fields [e.g., *Low*, 1997], a current sheet would form behind the CME when it propagates through the current sheet originally at the tip of the streamer, as indicated by the dashed line in Figure 1. Near solar minimum, slow solar wind would be confined to low latitudes associated with the streamer belt while fast solar wind comes from coronal holes at high latitudes [e.g., *McComas et al.*, 1998a]. The structured solar wind, as well as the increased plasma density around the preexisting current sheet which acts like an obstacle, would result in a concave-outward shape of the flux rope cross section. A simple relationship between the latitude θ of an observing spacecraft and the elevation angle δ of the flux rope normal can be obtained from the geometry,

$$\delta = \arcsin\left(\frac{R}{R_c}\sin\theta\right), \tag{1}$$

where R is the heliocentric distance of the spacecraft and R_c is the radius of curvature of the flux rope cross section. The radius of curvature is defined to be positive when the cross section is convex outward and negative when concave outward. An inverse correlation between δ and θ is indicated by Figure 1 for a concave-outward curvature, i.e., $\delta < 0$ when $\theta > 0$ and $\delta > 0$ when $\theta < 0$. We look at the normal elevation angle distributed over latitude for MCs near solar minimum in paper 1; a least squares fit of equation (1) to the data then gives an average radius of curvature of about -0.3 AU at 1 AU. Note that using this

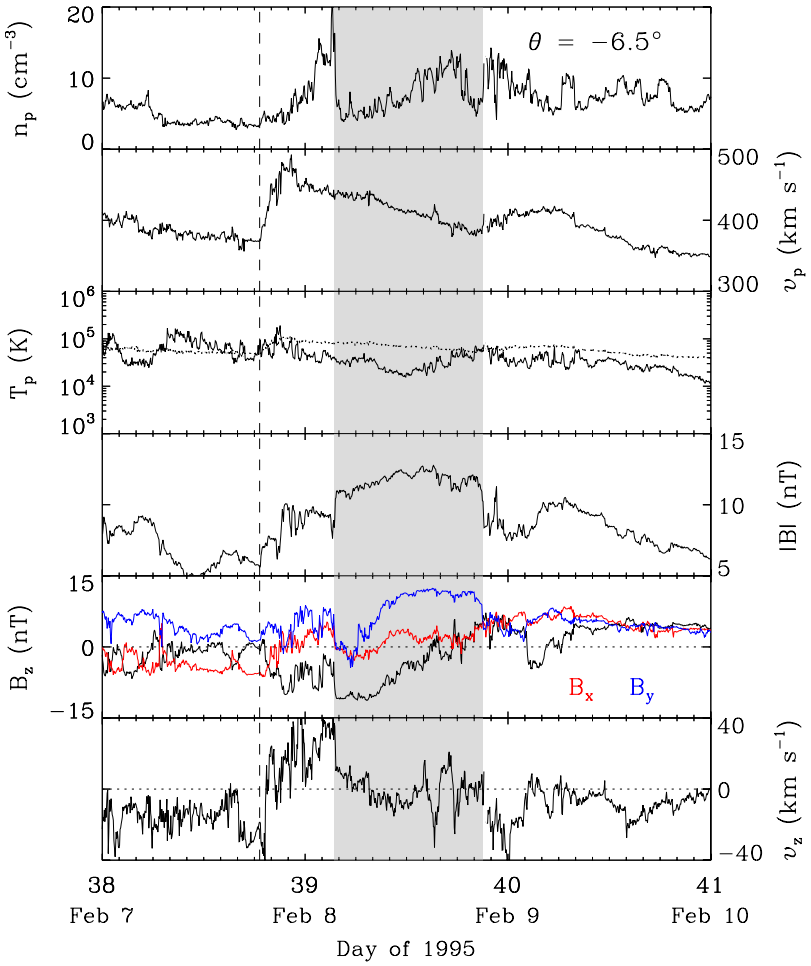

Figure 2. Solar wind plasma and magnetic field parameters measured by Wind across a typical MC (shaded region) near solar minimum. From top to bottom, the panels show the proton density, bulk speed, proton temperature, magnetic field strength and components, and the meridional velocity. The dashed line indicates the arrival time of the MC-driven shock. Dotted lines denote the expected proton temperature (third panel) and the zero levels of the field components (fifth panel) and the meridional flow (bottom panel). The latitude of Wind is given in the top panel.

relationship to obtain the curvature explicitly assumes a small deviation of the heliospheric current sheet from the equatorial plane (see discussion in section 4.1).

[6] The relative velocity (v_{re}) between an MC and the ambient solar wind (incoming flows with respect to the MC) is presumably along the radial direction and thus should be above the direction of the normal, if the MC is concave outward. By intuition, the plasma upstream of the MC would be deflected toward the equatorial plane (v_{de}) as shown in Figure 1; subsequent plasma accumulation ahead of the MC may force the flow to change direction and move poleward if the plasma is not removed efficiently from there (say, by lateral deflection in the equatorial plane). If the meridional flow indeed moves toward the equatorial plane, there would be an inverse correlation between the spacecraft latitude and the deflection flow direction as indicated in Figure 1. If the MC cross section is convex outward, then the upstream plasma would be deflected to high latitude and divert around the MC; in this case the spacecraft latitude is positively correlated with both the deflection flow direction and the elevation angle of the MC normal. We will test these points by looking at the deflection flow in the context of the MC curvature inferred from the normal elevation angle. Note that the flow deflection can only occur in the absence of substantial magnetic reconnection between the ambient and ICME fields, in which case the ambient flow cannot penetrate into ICMEs. Also note that a preceding shock may form if the ICME speed relative to the background solar wind is larger than the fast mode speed. Since the normal component of the solar wind flow in the shock frame is preferentially decreased across a fast mode shock compared with the tangential component, the ambient flow would change direction across the shock; the flow deflection by the shock may give rise to a flow reversal in the ICME sheath (a shocked region between the shock and ICME; see Figure 2) as predicted by *Manchester et al.* [2005]. The flow deflection by ICMEs should be separated from the shock deflection in studying the ICME curvature.

[7] Flow deflection can also occur in the equatorial plane. *Gosling et al.* [1987] find that the ambient plasma is preferentially deflected westward by ICMEs with a magnitude of ~25 km s^{-1} as a consequence of solar rotation. We

Table 1. Estimated Parameters of Magnetic Clouds at Wind for the Curvature Study

Date	Shock DOY	Start DOY	End DOY	θ^a (°)	δ^b (°)	$v_z{}^c$ (km s^{-1})	Θ^d (°)	Φ^d (°)
8 Feb 1995	38.78	39.15	39.88	−6.46	18.18	23.74 ± 13.06	−7.30 (−3.75)	284.85 (263.72)
22 Aug 1995	234.54	234.89	235.80	6.93	−24.43	−20.89 ± 6.17	−14.58 (−7.01)	279.49 (268.07)
18 Oct 1995	291.45	291.80	293.03	5.56	6.32	18.31 ± 14.04	−3.92 (−16.93)	284.08 (287.19)
1 Jul 1996	–	183.73	184.40	3.01	−20.65	−20.73 ± 10.45	7.26 (4.82)	100.58 (102.95)
10 Jan 1997	10.03	10.21	11.09	−4.13	2.47	31.24 ± 12.88	−22.50 (−28.48)	243.89 (240.19)
10 Feb 1997	40.53	41.12	41.75	−6.60	52.09	40.51 ± 11.67	22.72 (14.40)	315.13 (316.00)
15 May 1997	135.05	135.36	136.02	−2.56	−15.45	30.80 ± 20.67	−21.60 (−14.91)	110.07 (111.57)
16 May 1997	–	136.28	136.56	−2.46	11.15	8.89 ± 3.77	−21.79 (4.29)	290.15 (268.72)
3 Aug 1997	–	215.58	216.05	5.98	−4.54	−7.48 ± 6.10	2.37 (9.54)	33.88 (86.59)
1 Oct 1997	–	274.48	275.93	6.67	−45.04	−35.34 ± 26.06	−27.07 (11.49)	318.56 (315.00)
10 Oct 1997	283.66	283.92	285.02	6.10	14.70	31.67 ± 19.42	−7.72 (−18.05)	262.52 (255.49)

[a]Heliographic latitude of Wind.
[b]Elevation angle of the magnetic cloud (MC) normal with respect to the solar equatorial plane, estimated from minimum variance analysis (MVA).
[c]Meridional flow velocity ahead of the MCs in GSE coordinates (deflection by MCs instead of shocks).
[d]Axis elevation angle with respect to the solar equatorial plane and azimuthal angle in GSE coordinates, estimated from MVA (outside parentheses) and the GS method (inside parentheses).

look at the meridional deflection flow which is perpendicular to the ecliptic plane. The meridional flow can lead to a magnetic field component along the north-south direction, since the magnetic field is frozen-in with the plasma. The creation of the meridional field component is in nature equivalent to the magnetic field draping (see Figure 1) around ICMEs suggested by *Gosling and McComas* [1987] and *McComas et al.* [1988]. Note that the ambient field orientation shown in Figure 1 is highly idealized; in reality, it should depend on the deflection flow pattern. At the dayside magnetopause of the Earth, a southward magnetic field can result in a significant dawn-dusk electric field ($-\mathbf{v}_r \times \mathbf{B}_s$, where $\mathbf{v}_r$ is the radial velocity and $\mathbf{B}_s$ is the southward field), which controls the magnetic reconnection rate and hence generation of geomagnetic storms [*Dungey*, 1961]. *Russell et al.* [1974] show that the electric field must exceed 2 mV m^{-1} in order to produce a geomagnetic storm; since ICME sheaths are often associated with a large speed, this condition can be easily met. Observations have shown that the sheath region can be as geoeffective as ICME themselves [e.g., *Tsurutani et al.*, 1988].

[8] The strength of the meridional field is likely proportional to the magnitude of the meridional deflection flow; correlation between the deflection flow and ICME speeds is also expected. Therefore, the strength of the meridional field may be predictable based on observed CME speeds, which is of importance for space weather forecasting. Previous work has shown a correlation between CME/ICME speeds and the total field magnitude in ICME sheaths [*Lindsay et al.*, 1999; *Owens et al.*, 2005], which can be attributed to compression of the ambient field controlled by ICME speeds. This paper will further show how much of the sheath field is oriented in the meridional direction, in addition to the study of MC curvature. Sections 2 and 3 demonstrate how the meridional deflection flow indicates ICME curvature and sheath geoeffectiveness, respectively. We summarize and discuss the results in section 4.

2. Deflection Indicating Curvature

[9] Our curvature study focuses on MCs near solar minimum when the solar wind speed has a latitudinal dependence. We require MCs with axes close to the solar equatorial plane and not aligned with the radial direction, in order to see the most prominent effect of the cross-sectional curvature. In paper 1, we identified 14 MCs from solar wind plasma and magnetic field measurements by Wind between 1995 and 1997; all of these events have axes within 30 of the equatorial plane and more than 30 away from the radial direction. Events with leading edge speed smaller than or comparable to the ambient speed are discarded in this study, which leaves 11 MCs. A minimum variance analysis (MVA) of the measured magnetic fields within the MCs was used in the previous work to estimate the axis orientation and the MC normal. The covariance matrix of the magnetic field has eigenvectors corresponding to the maximum, intermediate and minimum variance directions [e.g., *Sonnerup and Cahill*, 1967; *Sonnerup and Scheible*, 1998]. The normal of a flattened MC is along the minimum variance direction; the intermediate variance direction is considered as the axis orientation due to nonuniform distribution of the axial fields over the flux rope cross section [e.g., *Burlaga and Behannon*, 1982; *Bothmer and Schwenn*, 1998]; the maximum variance direction would be along the azimuthal direction of a flux rope since the azimuthal field changes sign across the flux rope. The eigenvalues in the variance analysis are clearly separated for all of these events, so the variance directions are well determined. We also evaluate the axis orientation using the Grad-Shafranov (GS) technique [*Hau and Sonnerup*, 1999; *Hu and Sonnerup*, 2002] to make a comparison with the variance analysis. The GS technique yields the axis orientation in assessing the single-valued behavior of the thermal pressure and the axial field over a two-dimensional (2-D) vector potential, an advantage given by MHD quasi-equilibrium and the translational symmetry along the flux rope.

[10] Figure 2 shows a typical MC (the first event in Table 1) which is associated with a meridional deflection flow. Its boundaries can be readily determined from the strong magnetic field and smooth rotation of the field. The large rotation of the B_z component, combined with a small B_x, suggests a crossing of the spacecraft close to the MC axis. A depressed proton temperature is also apparent, compared with the expected temperature calculated from the observed

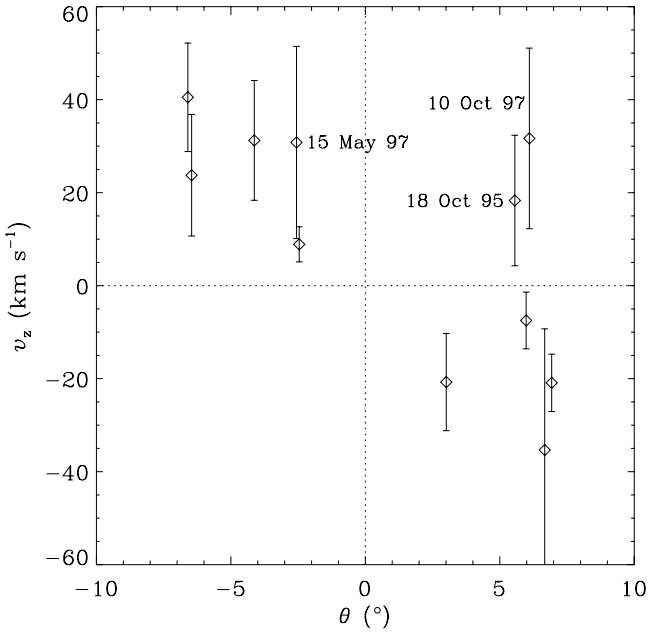

Figure 3. Meridional velocity ahead of the MCs in Table 1 as a function of Wind's heliographic latitude. The events dated as 18 October 1995 and 10 October 1997 are associated with positive normal elevation angles at $\theta > 0$ (as well as positive deflection flows), suggestive of a convex-outward curvature. The MC of 15 May 1997 does not have a coherent deflection flow and normal elevation angle.

speed using the method of *Lopez* [1987]. Within the sheath region, bounded by the preceding shock and the MC leading edge, the meridional velocity first drops to -40 km s^{-1}, presumably due to the directional change at the shock; flow deflection by shocks is often very brief, as illustrated in Figure 2. The meridional flow then reverses its direction and is as high as 40 km s^{-1} close to the MC. At the MC leading edge the meridional flow decreases abruptly and then fluctuates around the zero level inside the MC. The Wind spacecraft crossed the MC at a latitude of about $-6.5°$ (below the solar equatorial plane), where it observed a positive (northward) deflection flow right ahead of the MC, so the plasma upstream of the MC is deflected toward the equatorial plane (i.e., into the path of the MC propagation) instead of diverting around the MC. The MC normal has a positive elevation angle ($\delta \simeq 18°$; see Table 1), which implies that the MC cross section is concave outward. The concave-outward curvature and the equatorward deflection flow seem consistent with the picture depicted by Figure 1. Note that a considerable negative (southward) B_z occurs in the sheath and is coincident with the positive deflection flow. The southward field is probably induced by the deflection flow (if the plasma and magnetic field are frozen-in together) and will make the sheath geoeffective.

[11] Table 1 lists the 11 MCs and their parameters for the curvature study. The shock arrival time and the start and end of the MCs are given in a fractional day of year (DOY). The elevation angle of the MC normal (δ) is estimated from the MVA of the normalized magnetic fields within the MCs in GSE coordinates (in which **x** points from the Earth to the Sun, **z** is perpendicular to the ecliptic plane and points to the north, and **y** completes the right−handed triad), and is then rotated into a heliographic frame. The meridional flow (v_z) is estimated using an interactive program that selects an interval (by eyes) covering the maximum meridional speed. These intervals are often of a few hours ahead of the MCs; for comparison, ICME sheath regions are of 14 h on average when shocks are present [*Liu et al.*, 2006b]. Note that flow deflection by shocks is avoided by the interval selection. Averages and standard deviations of the meridional speed are then taken for the selected intervals. The MVA also yields the elevation angle (Θ) and azimuthal angle (Φ) of the MC axis orientation, which can be compared to the estimates from the GS technique. The axis elevation angle is given with respect to the solar equatorial plane while the azimuthal angle in GSE coordinates; all the MCs listed here have axes close to the equatorial plane and more than 30° away from the Sun−spacecraft direction, suitable for the curvature study. It is clear that these MCs near solar minimum generally have an inverse relationship between θ and δ, as originally reported in paper 1 (11 out of 14 if no events discarded). An inverse correlation is also apparent between θ and v_z for most of these events (9 out of 11, but see discussion below). These relationships reflect the curvature of the MC cross section resulting from the distortion by the ambient solar wind.

[12] Figure 3 displays the meridional velocity ahead of these MCs (i.e., MC deflection since shock deflection is excluded), with error bars indicating the standard deviation for the selected interval. The events of 18 October 1995, 15 May 1997, and 10 October 1997 were considered as exceptions in paper 1, which have a normal elevation angle positively correlated with the spacecraft latitude (i.e., δ and θ have the same sign; see Table 1); a positive correlation between δ and θ indicates a convex-outward curvature (i.e., $R_c > 0$), as shown by equation (1). As discussed in section 1, the upstream plasma will be deflected toward high latitude if the MC cross section is convex outward; the deflection flow ahead of the events of 18 October 1995 and 10 October 1997 is positive at $\theta > 0$ and confirms the convex-outward curvature inferred from the normal elevation angle. The poleward deflection ahead of the convex-outward MCs is in agreement with the finding of *Owens and Cargill* [2004]. The 15 May 1997 MC has a deflection flow which does not agree with the curvature indicated by the relationship between θ and δ (see Table 1). This MC is associated with an increasing speed profile across the event (not decreasing as usually seen in ICMEs), suggestive of a high-speed stream compressing the MC from behind; this stream interaction may explain the behavior of the deflection flow and the normal elevation angle. For the remaining eight events, we see an inverse correlation between v_z and θ as well as an inverse relationship between δ and θ (see Table 1); the inverse relationship between δ and θ implies a concave-outward structure while the inverse correlation between v_z and θ indicates equatorward flow deflection, similar to the scenario illustrated by Figure 1. The majority of the MCs (10 out of 11) have meridional deflection flows which appear intuitively consistent with the curvature inferred from the normal elevation angle at a certain latitude. Comparison with MHD simulations, however, is

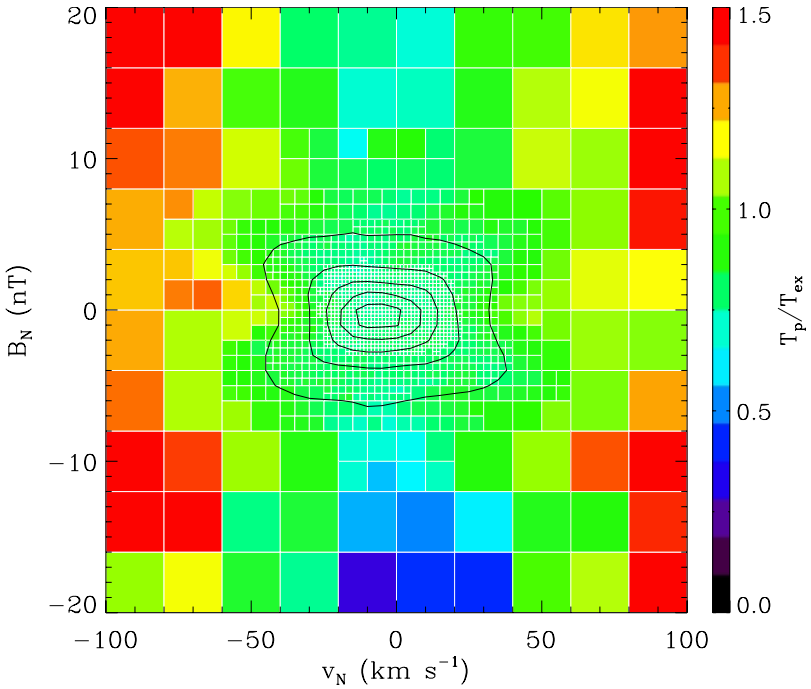

Figure 4. ACE measurements of the normalized proton temperature over the meridional velocity and the meridional field components (in RTN coordinates) for all the solar wind. Bins are smaller in regions with dense measurements while each bin contains at least 1000 data points. The color shading indicates the average value of T_p/T_{ex} within the bins. Black contours show the 2-D histogram of the data distribution at levels of [0.1, 0.3, 0.5, 0.7, 0.9].

needed in evaluating the flow deflection by the concave-outward MCs.

3. Deflection Indicating Geoeffectiveness

[13] The magnetic field is frozen into the interplanetary plasma due to the high electrical conductivity, so the meridional deflection flow will produce a meridional field component. The strength of the meridional field is expected to be proportional to the magnitude of the meridional flow. In this section, we look at the meridional field associated with the deflection flow in the sheath of fast ICMEs and compare it to the solar wind level.

3.1. Overview of the Solar Wind Meridional Flow

[14] Figure 4 shows a comprehensive view of the solar wind meridional flow and magnetic field. The 64 s averages of ACE SWEPAM [*McComas et al.*, 1998b] and MAG [*Smith et al.*, 1998] data between 1998 and 2005, containing about 3.3×10^6 spectra, are binned into cells over the 2−D plane of B_N and v_N (in RTN coordinates where **R** points from the Sun to the spacecraft, **T** is parallel to the solar equatorial plane and points to the planet motion direction, and **N** completes the right-handed system). Bins with dense data points are further subdivided, so the data distribution can be seen from the size of the cells as well as the black contours. Note that the expected temperature, T_{ex}, is essentially the typical temperature for normal solar wind given the observed speed. Figure 4 reveals interesting results about the production of the meridional field component. First, B_N seems to increase with v_N, as can be seen from the shape of the outermost contour (the 0.1 level); the four corners of the outmost contour protrude compared with the waists. Second, the hot plasma with $T_p/T_{ex} > 1$ is preferentially associated with a large v_N and B_N (i.e., at the corners of the plot); the high temperature is probably driven by stream interactions. Stream interaction regions (including ICME sheaths) should be hence geoeffective due to the large B_N's, as is well known. Third, the ICME plasma, characterized by $T_p/T_{ex} \leq 0.5$ [e.g., *Richardson and Cane*, 1995] (but note the average effect in Figure 4), shows a low v_N but high B_N, so the large B_N is intrinsic to the ICME plasma (i.e., not produced by the meridional flow). The ICME plasma seems to favor a southward (negative) field for the time period of 1998–2005; this south-north asymmetry is probably associated with the orientation of ICMEs for a specific solar cycle. Fourth, the most probable state of the solar wind has $v_N < 0$ and $B_N < 0$, as shown by the innermost contour; whether there is a solar cycle dependence is yet to be studied.

[15] The trend that B_N increases with v_N is also shown in Figure 5. The meridional speed, typical for the normal solar wind as restricted by $0.9 \leq T_p/T_{ex} \leq 1.1$, is binned into 5 km s^{-1} intervals; averages and standard deviations are then taken for the meridional speed and the meridional field magnitude over the bins. A linear trend is apparent up to 80 km s^{-1}, and then the data level off. Note that the majority of the data have $|v_N| < 50$ km s^{-1} (see Figure 4). It is not clear whether the flattening effect is spurious or associated with transient structures in the solar wind. The overall fit of the data, obtained with a least squares analysis, gives $B_N = 0.04 v_N$ (km s^{-1}) +1.9 nT. This linear increase arises from the fact that the field is frozen into the plasma,

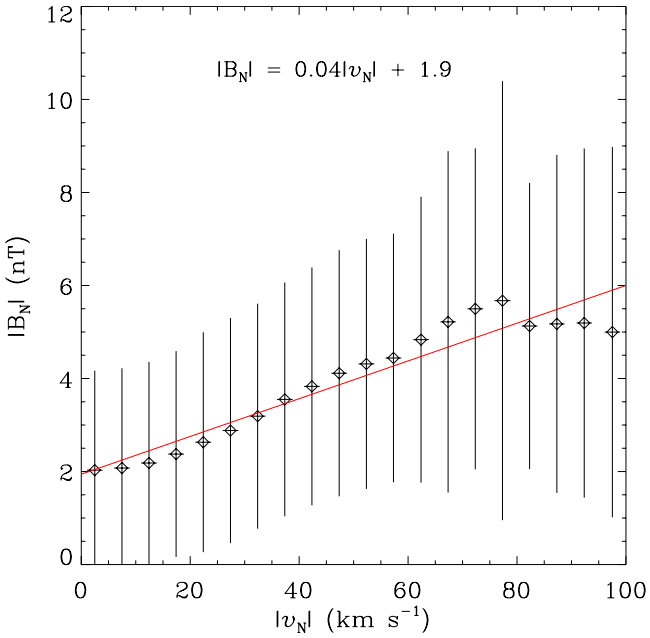

Figure 5. Solar wind meridional field magnitude as a function of the meridional speed. The horizontal and vertical bars indicate the standard deviations of the meridional speed and field within the bins, respectively. Also shown are the best fit of the data (solid line) and the fit parameters (text). Only the normal solar wind is included, as restricted by $0.9 \leq T_p/T_{ex} \leq 1.1$.

but a field magnitude of 1.9 nT cannot be accounted for by the meridional flow of the normal solar wind.

3.2. Deflection Ahead of Fast ICMEs

[16] A similar relationship may exist ahead of ICMEs. We look at sheath regions of fast ICMEs preceded by a shock in order to exclude the contamination effect of the ambient solar wind. ICMEs used in the study are from the survey of *Liu et al.* [2005]. Events with $T_p/T_{ex} \leq 0.5$ and $n_\alpha/n_p \geq 0.08$ were identified as ICMEs, where n_α is the density of alpha particles; the criteria yielded 54 ICMEs with preceding shocks from ACE data between 1998 and 2005. ICME boundaries are carefully readjusted by incorporating magnetic field signatures. All the shocks upstream of these ICMEs are fast-mode shocks across which the magnetic field increases. We do not differentiate between MCs and non-MC ICMEs, since the deflection flow should occur in all these sheaths. An interactive program is again used to select an interval in the sheaths covering the maximum of the deflection flow close to the ICME leading edge (shock deflection excluded); averages and standard deviations are calculated for v_N and B_N in the selected interval. The sheath regions are often turbulent, and temperature anisotropy instabilities may occur as in planetary magnetosheaths [*Liu et al.*, 2006b, 2007a]. The underlying flow and field configuration may be blurred by the superposed turbulence and wave activity. We require that the standard deviations of the meridional speed and field be smaller than the corresponding averages. The number of ICMEs is then reduced to 28.

[17] Figure 6 shows the correlation between the meridional field and deflection flow in the ICME sheaths. Data for the MCs used in the curvature study are also displayed. The meridional flow speed is up to 80 km s^{-1} and can induce a meridional field of ~20 nT, comparable to or even larger than the field magnitude as often seen within MCs. The linear correlation coefficient r_L is about 0.66 for the overall data as compared with Spearman's rank correlation coefficient $r_S \simeq 0.56$; the linear correlation coefficient is a measure of the linearity, whereas Spearman's correlation coefficient can quantify the significance of the correlation by reducing the effect of outlying points. The best fit gives $B_N = 0.19v_N + 1.5$ nT, clearly larger than the solar wind level obtained above. Interestingly, the field magnitude when $v_N = 0$ is comparable to the solar wind value, but the slope of the fit is much larger than the solar wind level (see Figure 5). Shock compression leads to a large magnetic field in the sheath region; the meridional field, once created by the meridional flow, can be enhanced by the field compression. This effect is similar to the amplification of the meridional field by converging radial flows perpendicular to the field found by *Manchester et al.* [2005]. Note that the Wind data near solar minimum are at the lower left corner of the plot, which may imply a solar cycle dependence of the deflection flow.

[18] Since the deflection flow results from a fast ICME moving through the solar wind, one may expect that the faster an ICME travels relative to the ambient medium, the larger the deflection flow is. The meridional speed is shown

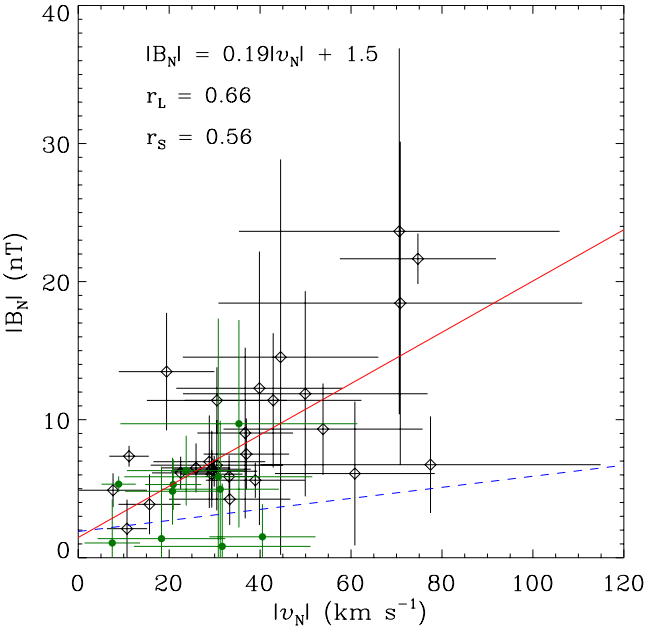

Figure 6. Meridional field magnitude as a function of the meridional speed in interplanetary coronal mass ejection (ICME) sheaths observed at ACE (diamonds) and ahead of Wind MCs used for the curvature study (filled circles). The horizontal and vertical bars indicate the standard deviations of the speed and field, respectively. Also shown are the best fit of the data (solid line), the solar wind level (dashed line), the fit parameters and the correlation coefficients between v_N and B_N (text).

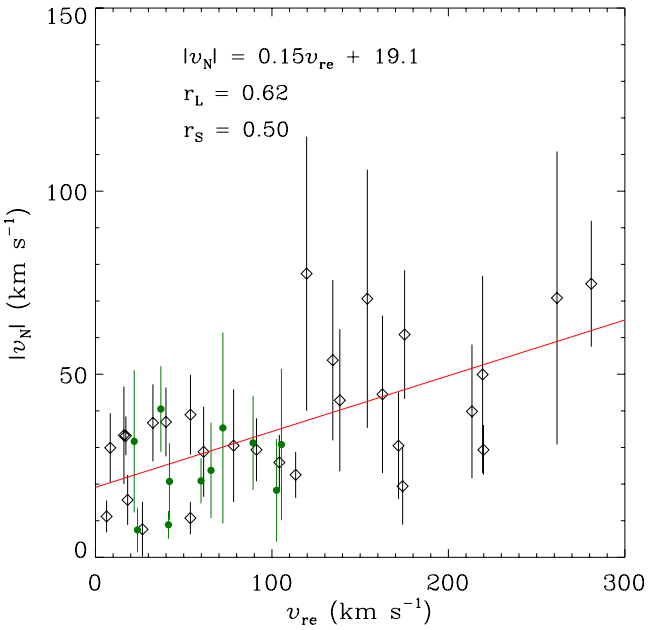

Figure 7. Meridional speed ahead of ICMEs as a function of the relative speed between ICME leading edge and the ambient solar wind. Same format as Figure 6.

in Figure 7 as a function of ICME leading-edge speed with respect to the ambient solar wind, v_{re}. A linear fit to the speed profile across the ICME interval is used to estimate the leading-edge speed; the ambient speed is obtained typically from the 5 h average upstream of the forward shock. The linear trend, with $r_L = 0.62$ and $r_S = 0.50$, is manifest in the data; the best fit is $v_N = 0.15v_{re} + 19.1$ km s^{-1}. As the meridional field is tightly bound to the meridional flow, a similar relationship is expected for B_N and v_{re}, which is made clear by Figure 8. We obtain a linear fit with $r_L = 0.68$ and $r_S = 0.61$

$$B_N = 0.05v_{re} + 3.2 \text{ nT}, \quad (2)$$

where v_{re} is in units of km s^{-1}. This expression is in agreement with the linear fits shown in Figures 6 and 7. Again, Wind data for the curvature study are also included and occupy the lower left corner of Figures 7 and 8.

[19] A similar relationship is reported between v_{re} and the average total field strength in sheath regions of MCs by *Owens et al.* [2005]; the gradient is the same as equation (2), but the intercept at $v_{re} = 0$ is higher (see Figure 8), so other field components are not negligible. The correlation between v_{re} and the total field in MC sheaths is simply an outcome of compression controlled by the relative speed. Interestingly, *Gonzalez et al.* [1998] find a similar correlation (the same slope) between the maximum total field and the maximum speed within MCs, which seems confirmed by *Lindsay et al.* [1999]. *Gonzalez et al.* [1998] suggest that this property may be intrinsic to MCs, somewhat related to CME initiation mechanisms. *Owens et al.* [2005], however, argue that it is more likely an effect of misidentification of the MC leading edge so that part of the sheath was included in the MC interval.

[20] The empirical relation expressed by equation (2) can foretell how much of the sheath field is oriented along the north-south direction if the ICME speed relative to the ambient solar wind is known. The ambient solar wind speed at 1 AU can be predicted by merged coronal and heliospheric MHD models using measured photospheric fields as input [e.g., *Odstrcil et al.*, 2002]. Coronagraph images of CMEs give the CME speed projected onto the sky, which is shown to be related to ICME speed as $v_{ICME} = 0.25v_{CME} + 360$ km s^{-1} acquired with a quadrature technique that reduces the projection effects [e.g., *Lindsay et al.*, 1999; *Gopalswamy et al.*, 2001]. With the observed CME speed and the predicted solar wind speed, equation (2) gives the sheath field along the meridional direction. Therefore, the empirical relation could be useful for space weather forecasting.

4. Summary and Discussion

[21] We combine the MC normal and the upstream meridional deflection flow to infer the shape of the MC cross section. Eight of 11 Wind MCs identified for the curvature study close to solar minimum have a normal elevation angle inversely correlated with the spacecraft latitude, indicative of a concave-outward curvature; the radius of curvature, obtained with a least squares analysis of equation (1), is ~ -0.2 AU for the eight events (as compared with -0.3 AU for 11 MCs estimated in paper 1). This radius of curvature is comparable to the average ICME radial width at 1 AU [e.g., *Liu et al.*, 2005, 2006a]. An inverse relationship is also observed between the upstream meridional flow and the spacecraft latitude for the 8 MCs, which suggests that the plasma right ahead of the

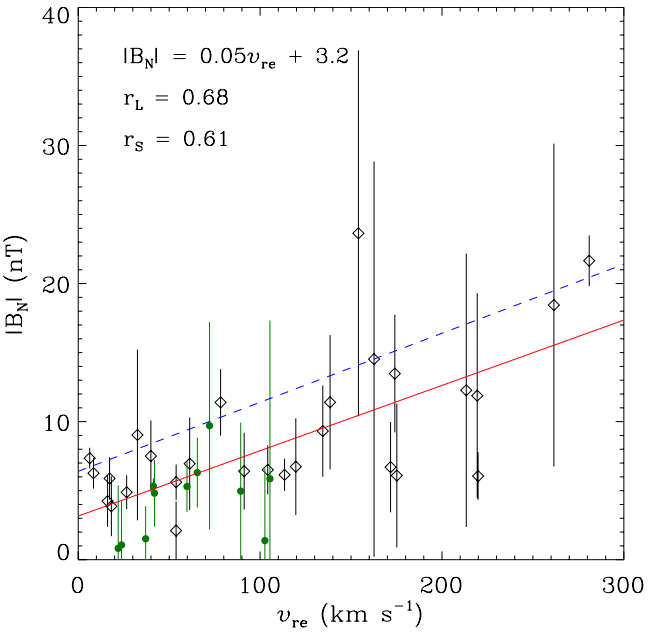

Figure 8. Meridional field ahead of ICMEs as a function of the relative speed between ICME leading edge and the ambient solar wind. The dashed line denotes a fit of $B = 0.05v_{re} + 6.4$ nT for the total field magnitude B in MC sheaths found by *Owens et al.* [2005]. Same format as Figure 6.

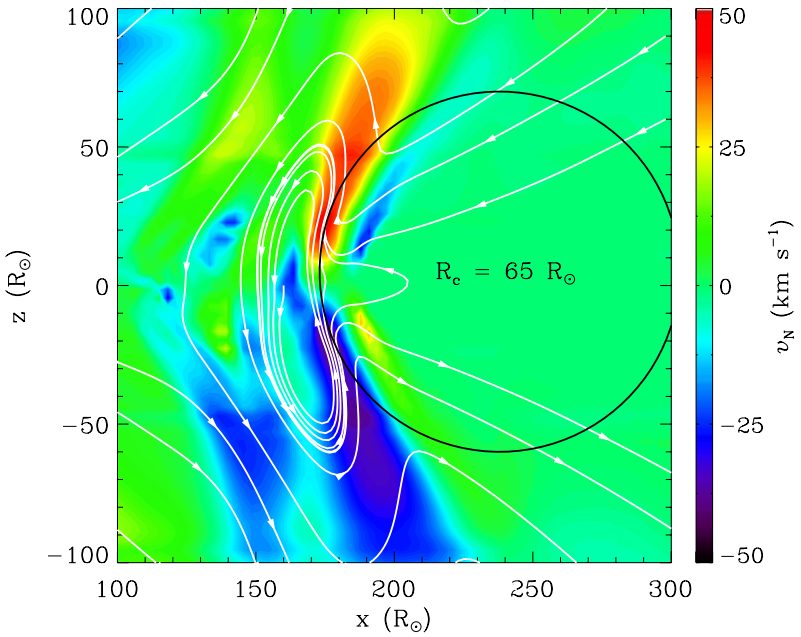

Figure 9. Cross section of the simulated CME in the meridional plane at 60 h after eruption. White lines indicate the magnetic field orientation. The color scale shows the meridional velocity (defined to be perpendicular to both the radial and longitudinal directions in order to compare with in situ data). The curvature of the CME is illustrated by a circle with a radius of R_c = 65 $R_\odot$, where $R_\odot$ is the radius of the Sun.

MCs is deflected toward the equatorial plane, in the way of MC propagation. Note that the converging flows may not produce a large accumulation of plasma in front of the MCs, since the plasma can be deflected laterally in the equatorial plane and/or jet outward if magnetic reconnection occurs (see discussion in section 4.2). Two of the remaining events (on 18 October 1995 and 10 October 1997, respectively) are likely convex outward, as indicated by both the elevation angle of the MC normal and the deflection flow. Only one event (on 15 May 1997) does not show a coherent behavior in its normal elevation angle and upstream flow deflection, which may be due to the presence of a high-speed stream behind the MC.

[22] *Owens* [2006] examined three MCs near solar minimum but did not find evidence of the concave-outward structure, which he ascribed to a sharp latitudinal transition from slow to fast wind that produces a flux rope concave outward globally but convex outward around the equatorial plane. An important point, missed by this argument, is that the preexisting heliospheric plasma sheet (HPS, a layer around the current sheet with increased mass density) acts like an obstacle and would be the main cause of the distortion at low latitudes. "V-arc" ICMEs similar to the picture shown in Figure 1 are observed recently by SMEI [*Kahler and Webb*, 2007]. The interaction between CMEs and the preexisting HPS, as well as the resulting concave-outward shape which closely resembles the structure shown in Figure 1, is clearly imaged by SECCHI and LASCO from the Sun out to several tens of solar radii [*Liu et al.*, 2008]. These coronagraph observations, together with our in situ measurements of the MC normal and MHD simulations (see below), provide compelling evidence for the concave-outward curvature of CMEs/ICMEs.

[23] The deflection flow can also be used to predict the geoeffectiveness of ICME sheaths. Linear relationships are observed between the meridional field and deflection flow in ICME sheaths, between the deflection flow and the ICME speed relative to the ambient solar wind, and between the meridional field and the relative ICME speed. On the basis of a global solar wind view, we show that these correlations are a consequence of the deflection flow controlled by the ICME relative speed and freezing the magnetic field with it. The meridional magnetic field can thus be predictable from the observed CME speed. A possible scheme to predict the sheath meridional field is given based on the derived empirical relationships.

4.1. Comparison With MHD Simulations

[24] We compare the results with MHD simulations of a CME propagating into a background heliosphere with a latitudinal speed gradient. *Manchester et al.* [2004] assume a specific heating function for the corona to reproduce the fast and slow solar wind at high and low latitudes, respectively; a flux rope CME is then launched from force imbalance and gains a final speed of 450 km s^{-1} in the solar wind. Figure 9 shows a cross-sectional view of the CME when it is ~170 $R_\odot$ away from the Sun. The model predicts a concave-outward curvature with a radius $R_c \sim 65$ $R_\odot$ (about 0.3 AU) near 1 AU, which is consistent with our estimate. A forward shock is discernable from the speed gradient and change of the field direction; the flow is first deflected to low latitude by the shock and then reverses direction in the sheath to move poleward. The poleward deflection ahead of the simulated CME is contrary to the results reported above, but the briefness of shock deflection as well as the flow reversal agrees with observations.

[25] *Odstrcil et al.* [2004] present MHD simulations of a density cloud (proxy of a CME) moving in an ambient solar wind; the ambient solar wind state is constructed by a coronal MHD model with observed photospheric magnetic fields as input. The plasma cloud is distorted into a concave-outward pancake with a radius of curvature ~0.1 AU (see their Figure 2). The distortion would be reduced by the field tension for ICMEs with embedded magnetic structure but not significantly since the flow momentum overwhelms the magnetic force. This model predicts a similar shock deflection (postshock confluence); the plasma in the density cloud moves away from the equatorial plane to high latitude, and as a result the meridional deflection flow ahead of the cloud cannot be separated from the plasma flow within the cloud (D. Odstrcil, private communication, 2008). Interaction of the cloud with a corotating interaction region in this model also complicates the interpretation. The above two models indicate that the ambient solar wind state is crucial in reproducing ICME propagation through the solar wind.

[26] A possibility to resolve the discrepancy between the observed and predicted deflection flows is that a concave-outward ICME may be directed to high latitude while extending to the equatorial plane so that the lower/higher end is sampled by a low-latitude spacecraft; if the upstream plasma is diverting around the obstacle, the spacecraft would see the flow as if it were toward the solar equatorial plane. In this case the normal elevation angle (δ), however, would have the same sign as the spacecraft latitude (θ), which conflicts with the observed inverse correlation between these two angles. Therefore, this possibility may not account for the statistical preference of equatorward deflection although it cannot be completely ruled out for an individual event.

[27] Also note that the picture described by Figure 1 is greatly idealized. The actual solar wind state at solar minimum is more complicated than suggested here. First, the solar wind speed minimum is not necessarily exactly at the heliographic equator for all longitudes near solar minimum. When the latitudinal deviation of the heliospheric current sheet is larger than the spacecraft latitude, interpretation of the relationship between θ and δ is more complicated. While this effect seems small as indicated by the observed preference of inverse correlation between θ and δ, caution has to be taken when examining individual events. Second, when the MC axis is not exactly in the equatorial plane it may be difficult to establish whether the observing spacecraft is above or below the MC axis. Third, other features (for example, another ICME) may be present nearby as an obstacle. All these factors would affect the determination of the curvature and thus the interpretation of the deflection flow. Follow-up studies with more events are needed to further assess the distortion effect on the plasma deflection. We leave the discrepancy between MHD simulations and our observations of the flow deflection as an open question.

[28] A closer look at Figure 9 also reveals that the meridional flows continue well into the flux rope, whereas there is often a clear discontinuity in the observed meridional flow at the leading edge of ICMEs as shown in Figure 2. The continuous meridional flow within the simulated CME seems to be caused by the limited numerical resolution. Further refinement on the grids is needed for the sheath region.

4.2. Implications for Sheath Dynamics

[29] If the equatorward deflection is true, antiparallel field lines will be pushed together by the flow confluence and magnetic reconnection is likely to occur (see Figure 1). Note that the magnetic reconnection is along the equatorial plane, different from the reconnection often seen in the dayside magnetopause. A reconnection jet may also be driven by the deflection inflows. Presumably, the upstream reconnection occurs everywhere along the ICME axis, so the reconnection jet would extend in the equatorial plane, forming a 2-D disk. The reconnection jet, if observed, will change our notion of how an ICME interacts with the ambient solar wind. The STEREO twin spacecraft are widely separated in longitude and are optimal for the observation of the 2-D jet. A search for the conjectured reconnection and jet from STEREO data is a future work.

[30] The meridional deflection flow also results in meridional magnetic fields, as demonstrated in section 3. Shock compression yields a large magnetic field and is often accompanied by converging flows, which can amplify the meridional field once induced by the meridional flow. ICME sheaths are therefore a particularly effective region in producing large meridional fields, which has important implications for generation of geomagnetic storms.

[31] ICME-driven shocks should bear a curvature similar to the ejecta. A dimple in the shock surface, resulting from propagation through the heliospheric plasma sheet, is studied by numerical simulations [e.g., *Odstrcil et al.*, 1996] and seems confirmed by in situ measurements of the shock normal [*Burton et al.*, 1992; J.C. Kasper and W.B. Manchester IV, Confirmation of equatorial dimples in solar minimum shock surfaces, submitted to Astrophysical Journal, 2008]. A lesson from Voyager 1 observations across the termination shock is that the flux of anomalous cosmic rays continues to increase across the shock [*Stone et al.*, 2005], which may be due to a topological effect of the shock leading to particle reacceleration in the heliosheath (in addition to shock acceleration). Similarly, velocity shear and turbulence generated by ICME and shock curvatures may give rise to a further acceleration of particles in ICME sheaths.

4.3. Prediction of the Meridional Field Direction

[32] Measuring the CME magnetic field days before CMEs reach the Earth is central to space weather forecasting but has been lacking. The empirical scheme proposed here is complementary to Faraday rotation measurements of the CME field using polarized radio signals [*Liu et al.*, 2007b]. While the empirical method gives the meridional field strength in ICME sheaths, the direction of the meridional field still needs to be determined. The sign of the meridional field would depend on both the interplanetary field and ICME orientations. *McComas et al.* [1989] suggest a draping model with which the direction of the meridional field can be predicted, given the inward/outward direction of the ambient radial field and whether the ICME is directed northward/southward of an observing spacecraft. They show that, for 13 of 17 events studied, the direction of the meridional field in ICME sheaths is correctly predicted. As

discussed above, draping of the ambient field around ICMEs is tied to the deflection flow, so the draping model can be used in combination with our empirical scheme in predicting the meridional field magnitude and direction. Turbulence and wave activity may overwhelm the underlying field configuration; a large scatter is also seen in Figure 6. Therefore, the method has to be used with great caution for real-time predictions.

[33] **Acknowledgments.** The research was supported by the STEREO project under grant NAS5-03131. We acknowledge the use of ACE and Wind data from the NSSDC and are grateful to the referees for their helpful suggestions. This work was also supported in part by grant NNSFC 40621003.

[34] Amitava Bhattacharjee thanks Helfried Biernat and another reviewer for their assistance in evaluating this paper.

References

Bothmer, V., and R. Schwenn (1998), The structure and origin of magnetic clouds in the solar wind, *Ann. Geophys.*, *16*, 1.

Burlaga, L. F., and K. W. Behannon (1982), Magnetic clouds — Voyager observations between 2 and 4 AU, *Solar Phys.*, *81*, 181.

Burlaga, L. F., E. Sittler, F. Mariani, and R. Schwenn (1981), Magnetic loop behind an interplanetary shock: Voyager, Helios, and IMP 8 observations, *J. Geophys. Res.*, *86*, 6673.

Burton, M. E., G. L. Siscoe, and E. J. Smith (1992), Shapes of strong shock fronts propagating through the coronal streamer belt, *J. Geophys. Res.*, *97*, 12,283.

Cid, C., M. A. Hidalgo, T. Nieves-Chinchilla, J. Sequeiros, and A. F. Viñas (2002), Plasma and magnetic field inside magnetic clouds: A global study, *Sol. Phys.*, *207*, 187.

Dungey, J. W. (1961), Interplanetary magnetic field and the auroral zones, *Phys. Rev. Lett.*, *6*, 47.

Gonzalez, W. D., et al. (1998), Magnetic cloud field intensities and solar wind velocities, *Geophys. Res. Lett.*, *25*, 963.

Gopalswamy, N., A. Lara, S. Yashiro, M. L. Kaiser, and R. A. Howard (2001), Predicting the 1-AU arrival times of coronal mass ejections, *J. Geophys. Res.*, *106*, 29,207.

Gosling, J. T., and D. J. McComas (1987), Field line draping about fast coronal mass ejecta: A source of strong out-of-ecliptic interplanetary magnetic fields, *Geophys. Res. Lett.*, *14*, 355.

Gosling, J. T., M. F. Thomsen, S. J. Bame, and R. D. Zwickl (1987), The eastward deflection of fast coronal mass ejecta in interplanetary space, *J. Geophys. Res.*, *92*, 12,127.

Groth, C. P. T., D. L. De Zeeuw, T. I. Gombosi, and K. G. Powell (2000), Global three-dimensional MHD simulation of a space weather event: CME formation, interplanetary propagation, and interaction with the magnetosphere, *J. Geophys. Res.*, *105*, 25,053.

Hau, L.-N., and B. U. Ö. Sonnerup (1999), Two-dimensional coherent structures in the magnetopause: Recovery of static equilibria from single-spacecraft data, *J. Geophys. Res.*, *104*, 6899.

Hidalgo, M. A., T. Nieves-Chinchilla, and C. Cid (2002), Elliptical cross-section model for the magnetic topology of magnetic clouds, *Geophys. Res. Lett.*, *29*(13), 1637, doi:10.1029/2001GL013875.

Hu, Q., and B. U. Ö. Sonnerup (2002), Reconstruction of magnetic clouds in the solar wind: Orientations and configurations, *J. Geophys. Res.*, *107*(A7), 1142, doi:10.1029/2001JA000293.

Kahler, S. W., and D. F. Webb (2007), V arc interplanetary coronal mass ejections observed with the Solar Mass Ejection Imager, *J. Geophys. Res.*, *112*, A09103, doi:10.1029/2007JA012358.

Kaiser, M. L. (2005), The STEREO mission: An overview, *Adv. Space Res.*, *36*, 1483.

Lepping, R. P., J. A. Jones, and L. F. Burlaga (1990), Magnetic field structure of interplanetary magnetic clouds at 1 AU, *J. Geophys. Res.*, *95*, 11,957.

Lindsay, G. M., J. G. Luhmann, C. T. Russell, and J. T. Gosling (1999), Relationships between coronal mass ejection speeds from coronagraph images and interplanetary characteristics of associated interplanetary coronal mass ejections, *J. Geophys. Res.*, *104*, 12,515.

Liu, Y., J. D. Richardson, and J. W. Belcher (2005), A statistical study of the properties of interplanetary coronal mass ejections from 0.3 to 5.4 AU, *Planet. Space Sci.*, *53*(3), doi:10.1016/j.pss.2004.09.023.

Liu, Y., J. D. Richardson, J. W. Belcher, J. C. Kasper, and H. A. Elliott (2006a), Thermodynamic structure of collision-dominated expanding plasma: Heating of interplanetary coronal mass ejections, *J. Geophys. Res.*, *111*, A01102, doi:10.1029/2005JA011329.

Liu, Y., J. D. Richardson, J. W. Belcher, J. C. Kasper, and R. M. Skoug (2006b), Plasma depletion and mirror waves ahead of interplanetary coronal mass ejections, *J. Geophys. Res.*, *111*, A09108, doi:10.1029/2006JA011723.

Liu, Y., J. D. Richardson, J. W. Belcher, C. Wang, Q. Hu, and J. C. Kasper (2006c), Constraints on the global structure of magnetic clouds: Transverse size and curvature, *J. Geophys. Res.*, *111*, A12S03, doi:10.1029/2006JA011890.

Liu, Y., J. D. Richardson, J. W. Belcher, and J. C. Kasper (2007a), Temperature anisotropy in a shocked plasma: Mirror-mode instabilities in the heliosheath, *Astrophys. J.*, *659*, L65.

Liu, Y., W. B. Manchester IV, J. C. Kasper, J. D. Richardson, and J. W. Belcher (2007b), Determining the magnetic field orientation of coronal mass ejections from Faraday rotation, *Astrophys. J.*, *665*, 1439.

Liu, Y., J. G. Luhmann, D. Odstrcil, Y. Li, A. Vourlidas, R. P. Lin, and S. D. Bale (2008), Initiation and evolution of CMEs from helmet streamers, *Eos Trans. AGU*, *89*(23), Jt. Assem. Suppl., Abstract SH31A-04.

Lopez, R. E. (1987), Solar cycle invariance in solar wind proton temperature relationships, *J. Geophys. Res.*, *92*, 11,1891987.

Low, B. C. (1997), The role of coronal mass ejections in solar activity, in *Coronal Mass Ejections, Geophys. Monogr. Ser.*, vol. 99, edited by N. Crooker, J. A. Joselyn, and J. Feynman, pp. 39, AGU, Washington, D. C.

Manchester, W. B., IV, T. I. Gombosi, I. Roussev, A. Ridley, D. L. De Zeeuw, I. V. Sokolov, K. G. Powell, and G. Tóth (2004), Modeling a space weather event from the Sun to the Earth: CME generation and interplanetary propagation, *J. Geophys. Res.*, *109*, A02107, doi:10.1029/2003JA010150.

Manchester, W. B., IV, et al. (2005), Coronal mass ejection shock and sheath structures relevant to particle acceleration, *Astrophys. J.*, *622*, 1225.

McComas, D. J., J. T. Gosling, D. Winterhalter, and E. J. Smith (1988), Interplanetary magnetic field draping about fast coronal mass ejecta in the outer heliosphere, *J. Geophys. Res.*, *93*, 2519.

McComas, D. J., J. T. Gosling, S. J. Bame, E. J. Smith, and H. V. Cane (1989), A test of magnetic field draping induced Bz perturbations ahead of fast coronal mass ejecta, *J. Geophys. Res.*, *94*, 1465.

McComas, D. J., et al. (1998a), Ulysses' return to the slow solar wind, *Geophys. Res. Lett.*, *25*, 1.

McComas, D. J., S. J. Bame, P. Barker, W. C. Feldman, J. L. Phillips, P. Riley, and J. W. Griffee (1998b), Solar Wind Electron Proton Alpha Monitor (SWEPAM) for the Advanced Composition Explorer, *Space Sci. Rev.*, *86*, 563.

Mulligan, T., and C. T. Russell (2001), Multispacecraft modeling of the flux rope structure of interplanetary coronal mass ejections: Cylindrically symmetric versus nonsymmetric topologies, *J. Geophys. Res.*, *106*, 10,581.

Odstrcil, D., M. Dryer, and Z. Smith (1996), Propagation of an interplanetary shock along the heliospheric plasma sheet, *J. Geophys. Res.*, *101*, 19,973.

Odstrcil, D., J. A. Linker, R. Lionello, Z. Mikic, P. Riley, V. J. Pizzo, and J. G. Luhmann (2002), Merging of coronal and heliospheric numerical two-dimensional MHD models, *J. Geophys. Res.*, *107*(A12), 1493, doi:10.1029/2002JA009334.

Odstrcil, D., P. Riley, and X. P. Zhao (2004), Numerical simulation of the 12 May 1997 interplanetary CME event, *J. Geophys. Res.*, *109*, A02116, doi:10.1029/2003JA010135.

Owens, M. J. (2006), Magnetic cloud distortion resulting from propagation through a structured solar wind: Models and observations, *J. Geophys. Res.*, *111*, A01105, doi:10.1029/2004JA010814.

Owens, M. J., and P. J. Cargill (2004), Non-radial solar wind flows induced by the motion of interplanetary coronal mass ejections, *Ann. Geophys.*, *22*, 4397.

Owens, M. J., P. J. Cargill, C. Pagel, G. L. Siscoe, and N. U. Crooker (2005), Characteristic magnetic field and speed properties of interplanetary coronal mass ejections and their sheath regions, *J. Geophys. Res.*, *110*, A01105, doi:10.1029/2004JA010814.

Richardson, I. G., and H. V. Cane (1995), Regions of abnormally low proton temperature in the solar wind (1965–1991) and their association with ejecta, *J. Geophys. Res.*, *100*, 23,397.

Riley, P., J. A. Linker, Z. Mikic, D. Odstrcil, T. H. Zurbuchen, D. Lario, and R. P. Lepping (2003), Using an MHD simulation to interpret the global context of a coronal mass ejection observed by two spacecraft, *J. Geophys. Res.*, *108*(A7), 1272, doi:10.1029/2002JA009760.

Riley, P., J. A. Linker, R. Lionello, Z. Mikic, D. Odstrcil, M. A. Hidalgo, C. Cid, Q. Hu, R. P. Lepping, B. J. Lynch, and A. Rees (2004), Fitting flux ropes to a global MHD solution: A comparison of techniques, *J. Atmos. Sol. Terr. Phys.*, *66*, 1321.

Russell, C. T., R. L. McPherron, and R. K. Burton (1974), On the cause of geomagnetic storms, *J. Geophys. Res.*, *79*, 1105.

Smith, C. W., J. L'Heureux, N. F. Ness, M. H. Acuña, L. F. Burlaga, and J. Scheifele (1998), The ACE Magnetic Fields Experiment, *Space Sci. Rev.*, *86*, 613.

Sonnerup, B. U. Ö., and L. J. Cahill Jr. (1967), Magnetopause structure and attitude from Explorer 12 observations, *J. Geophys. Res.*, *72*, 171.

Sonnerup, B. U. Ö., and M. Scheible (1998), Minimum and maximum variance analysis, in *Analysis Methods for Multi-Spacecraft Data*, edited by G. Paschmann and P. W. Daly, pp. 185, Int. Space Sci. Inst., Bern, Switzerland.

Stone, E. C., A. C. Cummings, F. B. McDonald, B. C. Heikkila, N. Lal, and W. R. Webber (2005), Voyager 1 explores the termination shock region and the heliosheath beyond, *Science*, *309*, 2017.

Tsurutani, B. T., E. J. Smith, W. D. Gonzalez, F. Tang, and S. I. Akasofu (1988), Origin of interplanetary southward magnetic fields responsible for major magnetic storms near solar maximum (1978–1979), *J. Geophys. Res.*, *93*, 8519.

Vandas, M., and E. P. Romashets (2003), A force-free field with constant alpha in an oblate cylinder: A generalization of the Lundquist solution, *Astron. Astrophys.*, *398*, 801.

S. D. Bale, R. P. Lin, Y. Liu, and J. G. Luhmann, Space Sciences Laboratory, University of California, Berkeley, CA 94720, USA. (liuxying@ssl.berkeley.edu)

W. B. Manchester IV, Center for Space Environment Modeling, University of Michigan, Ann Arbor, MI 48109, USA.

J. D. Richardson, Kavli Institute for Astrophysics and Space Research, Massachusetts Institute of Technology, Cambridge, MA 02139, USA.